# Catalytic disinfection: Quasi-dynamically monitoring bacteria sterilization based on CuNPs/ZnIn$_2$S$_4$ disinfectants and *in-situ* CuNPs regeneration

Zhong-Ting Hu [a,b,1], Yan-Fei Fei [a,1], Qiong-Yu Wang [a], Qi Zhao [c], Siew-Leng Loo [d], Mian Hu [a], Yonghe Li [b], Yujie Song [e], Jie-Xin Wang [f], Zhi-Gang Shen [g], Hua Sheng [c,*], Jiade Wang [a,*], Jincai Zhao [c]

[a] College of Environment, Zhejiang University of Technology (ZJUT), Hangzhou 310014, China
[b] Industrial Catalysis Institute of ZJUT, Hangzhou 310014, China
[c] Key Laboratory of Photochemistry, Institute of Chemistry Chinese Academy of Sciences, Beijing National Laboratory for Molecular Sciences, Beijing 100190, China
[d] School of Material Science and Engineering, Nanyang Technological University, Nanyang Avenue, 639798, Singapore
[e] Engineering Laboratory of Advanced Energy Materials, Ningbo Institute of Materials Technology & Engineering, Chinese Academy of Sciences, Ningbo 315201, China
[f] State Key Laboratory of Organic-Inorganic Composites and Research Center of the Ministry of Education for High Gravity Engineering and Technology, Beijing University of Chemical Technology, Beijing 100029, China
[g] School of Chemical Technology, Xiangtan University, Xiangtan, Hunan 411105, China

A R T I C L E  I N F O

A B S T R A C T

As a novel sterilization technology (*i.e.*, catalytic disinfection), a disinfectant with high efficiency, economy, safety, and/or long lifespan is sought, while the mechanism is to be revealed. Herein, compared with noble Ag, Cu adopted has successfully modulated CuNPs/ZnIn$_2$S$_4$ (Cu/ZIS) disinfectants *via* a green photodeposition at room temperature. The Cu/ZIS-driven catalytic disinfection under indoor lighting (Vis, $420 < \lambda < 630$ nm) exhibited excellent bactericidal efficiencies of 100% both for *P. aeruginosa* ($\geq 6$ logs) and mixed bacteria in natural water (*i.e.*, Dongtiaoxi River), while it also functions as hindering bacteria regrowth and suppressing Cu loss. The bacteria death process (*e.g.*, cell membrane damage, intracellular compounds leaching) was studied *via* quasi-dynamically monitoring and a new action mechanism of Cu/ZIS with *in-situ* regeneration of Cu atomic clusters was also uncovered. These results provide a cheap well-designed disinfectant with a long lifespan, and a feasibility of catalytic disinfection for harmful microorganisms.

## 1. Introduction

Water is a resource that human being depends on for survival in the long history of development. Nowadays, drug-resistant bacteria (DRB) are widespread in aqueous systems, posing great threats to human health [1,2]. The most harmful waterborne microorganisms can be removed/inactivated through conventional water treatment by combining physical adsorption/filtration with chemical disinfectants (such as chlorides and ozone), and even ultraviolet (UV) radiation [3,4]. However, the above methods have certain drawbacks including the formation of disinfection by-products (DBPs), high energy-consumption, and regrowth of bacteria [5,6]. Additionally, the outbreak of the Corona Virus Disease 2019 (COVID-19) across the globe, causes serious economic losses and human deaths, as well as the urgency on the development of effective disinfectants. According to the reports, the overuse of disinfectant drugs during the new COVID-19 pandemic can accelerate the production and spread of superbugs [7,8]. Hence, a novel disinfectant and its technology with high-efficiency, energy-saving, environmentally-friendly, economical, and multi-function is urgently needed.

Antibacterial materials, with high efficiency, safety, and long life-span, are considered as one of the most powerful and promising means in the field of disinfection [9–11]. Up to now, different types of functional materials have been extensively developed and gradually applied in water disinfection including typical TiO$_2$-based, graphene-based, Ag-based and S-based disinfectants [5]. Especially, noble Ag nanoparticles (AgNPs) exhibit excellent sterilization, water purification and antiseptic properties, and are gradually being employed in daily life [12,

---

* Corresponding authors.
*E-mail addresses:* hsheng@iccas.ac.cn (H. Sheng), jdwang@zjut.edu.cn (J. Wang).
[1] Co-first authors.

[13]. However, its high price and environmental toxicity have always attracted people's attention and hindered its broad-spectrum application [14]. Copper has been considered to have good antiseptic and antibacterial properties since ancient times, and is used in the preservation and treatment of water and food [15], as well as in medical hygiene [16]. In 2008, it was recognized as the first metallic antibacterial agent by the American Environmental Protection Agency (US EPA) [15]. The sterilization mechanism of Cu principally includes (1) the damage to the membrane of cells or viruses through direct contact with CuNPs, (2) the infiltration of Cu ions into cells, which induce an oxidative stress and disrupt RNA and DNA functions, (3) the generation of reactive oxygen species (ROSs) by release electrons of copper, leading to enzymatic or non-enzymatic mediated oxidative damage (including protein oxidation, lipid peroxidation, and even DNA damage) [17,18].

While Cu is less toxic than Ag, the latter has been more widely studied for its application in developing disinfection systems. The main reason for this difference is the loss of CuNPs due to the instability as a consequent of oxidation in air or aqueous media [19]. To address the stability of metal, manufacturing composite materials is one of the most effective strategies [20]. For instance, Villanueva et al. fabricated a starch hydrogel of silicon-coated CuNPs with antimicrobial activity[19]. Composites can also exhibit synergistic effects and enhance catalytic performance by combining the properties of the component phases to apply to environment disinfection, namely Ag-TiO$_2$ [21], Cu-TiO$_2$ [22], Ag-ZnO [13], CuO-Co$_2$O$_4$ [23]. Moreover, studies have shown that photogenerated electrons can function as a reducing agent, which can reduce metal ions to solid metal elements to achieve anchoring and regenerating of solid metal (*e.g.*, atomic clusters) [24]. As an advanced functional material, zinc indium sulfide (ZnIn$_2$S$_4$), a ternary sulfide, has recently attracted attention in the fields of aqueous treatment and energy production due to its remarkable chemical stability, visible-light absorption and good photoelectric-conversion properties [25,26]. Moreover, studies have pointed out that it has certain antibacterial properties through photocatalytic formation of ROSs [5]. Therefore, it should be a reasonable design when ZnIn$_2$S$_4$ works as a potential electron donor for *in-situ* reduction of metal ions (M$^{n+}$) through photocatalysis under visible-light irradiation and the separation efficiency of photogenerated electrons (e$^-$) and holes (h$^+$) pairs can be enhanced with less recombination [27,28].

Herein, an ingeniously designed disinfectant by photo-depositing CuNPs on ZnIn$_2$S$_4$ photocatalyst has been successfully obtained in the form of pseudo-homogeneous dispersion. The bacteria sterilization based on CuNPs/ZnIn$_2$S$_4$ (Cu/ZIS) solid disinfectants in water was quasi-dynamically monitored for the first time by systematic integrated analysis and characterization. The corresponding bactericidal mechanism was elucidated based on a novel concept proposed about *in-situ* regeneration of Cu atomic clusters by using photogenerated electrons. The achieved results revealed that Vis/Cu/ZIS disinfection system has remarkable bactericidal performance with a long lifespan not only for bacteria model in artificially-contaminated water but also for mixed bacteria in natural water.

## 2. Experimental section

### 2.1. Chemicals and materials

None of the chemicals used in this study were further purified. Zinc chloride (98%), copper chloride (98%), sodium phosphate monobasic dihydrate (AR grade), and sodium phosphate dibasic heptahydrate ($\geq$ 98%) were purchased from Macklin. Indium (III) chloride tetrahydrate (AR grade), sodium borohydride (AR grade), potassium chloride ($\geq$ 99.5%), sodium chloride ($\geq$ 99.8%), thioacetamide ($\geq$ 99.0%), isopropanol alcohol ($\geq$ 99.7%, IPA), 5,5-dimethyl-1-pyrroline-*N*-oxide (DMPO), 2,2,6,6-Tetramethyl-1-piperidinyloxy (98.0%, TEMPO), and ethanol ($\geq$ 99.5%) were ordered from Sinopharm Chemical Reagent Co., Ltd. Cupric chloride anhydrous (98%, Adamas-beta). Tryptic soy broth (TSB) and tryptone soy agar (TSA) were purchased from Hopebiol. All of the experiments used Milli-Q ultrapure water (18.2 MΩ·cm$^{-1}$).

### 2.2. Bacterial strains

Model bacteria used are Gram-negative *Pseudomonas aeruginosa* (*P. aeruginosa*) (ATCC27853) and *Escherichia coli* (*E. coli*) (ATCC25922). All bacterial strains were conventionally sustained in TSB with 25% glycerol at $-$ 80 °C.
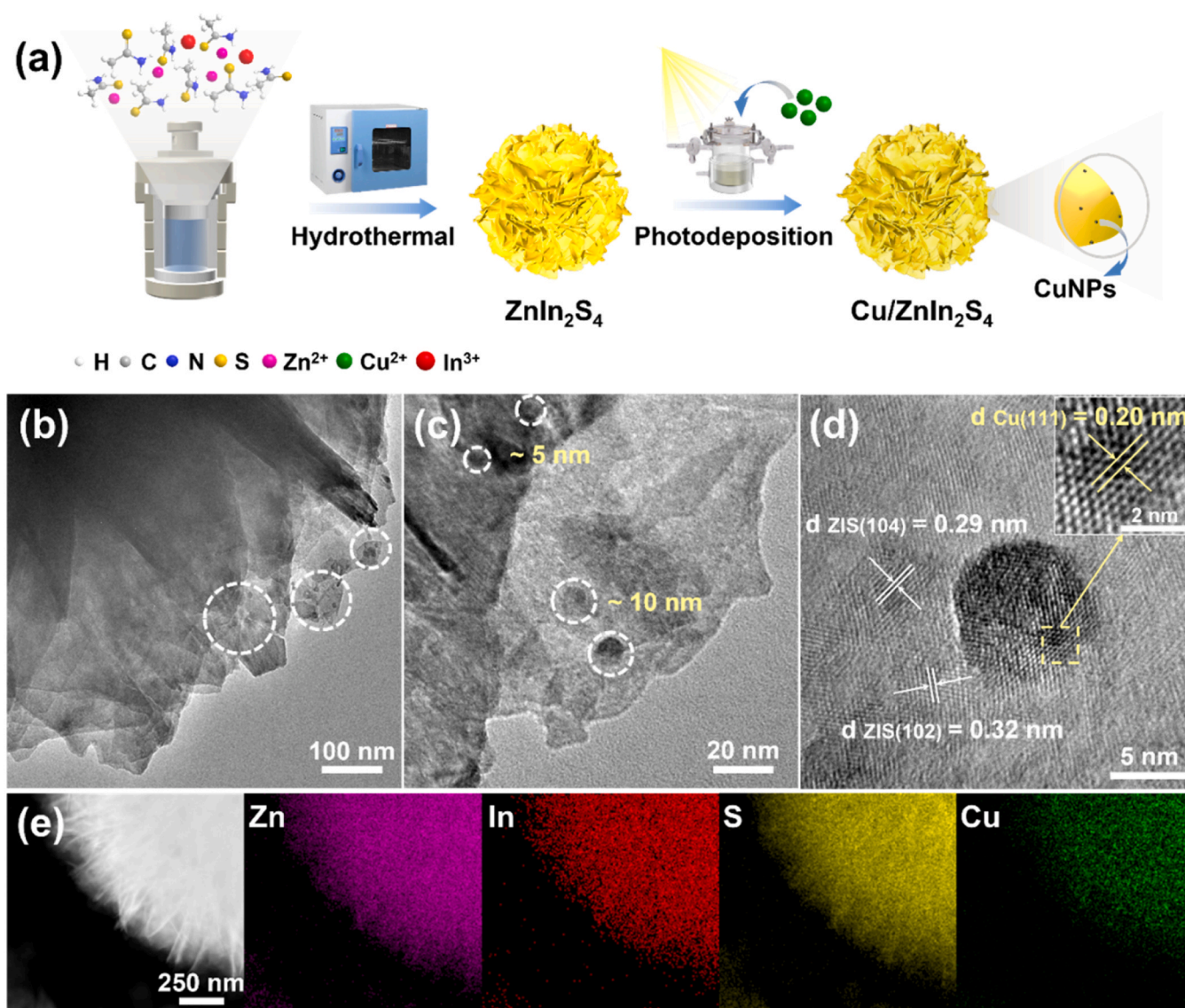
### 2.3. Preparation of disinfectants

The materials preparation process is described in detail in the Supporting Information. As our work previously, the hierarchical structure ZnIn$_2$S$_4$ (ZIS) catalyst was prepared using a simple hydrothermal way [29]. The finally product (achieved at 160 °C for 16 h in autoclave reactor) dried in a vacuum oven (60 °C, 12 h) to obtain the ZIS powder. Cu-decorated ZIS nanocomposites were fabricated by a photochemical deposition way [24]. In a typical operation, 100 mg of the ZIS was suspended in MQ water (45 mL) with the addition of varied precalculated amount of CuCl$_2$. To completely remove the oxygen both in the suspension and quartz reactor, it was bubbled with N$_2$ for 15 min. Then, the solution was kept stirring magnetically during visible-light illumination (420 < λ < 630 nm) before adding the precalculated amount of NaBH$_4$ to accelerate the reduction process of Cu ions to metallic copper on the surface of ZIS. After 1 h, Cu nanoparticles (CuNPs) could be successfully anchored on the surface of ZIS. The collected product was washed with a water/ethanol solvent and dried in a vacuum oven at 60 °C all night. As comparison experiments, the Cu/ZIS nanocomposites with different ratios (0.5%, 1.0%, 2.0%, and 10%) of CuNPs by weight were prepared individually.

### 2.4. Characterization

The achieved samples were characterized in detailed comprehensively by a variety of characterization techniques. Field emission scanning electron microscopy (FE-SEM, Zeiss, Gemini 500) and transmission electron microscopy (TEM, FEI, Tecnai G2 F30 S-Twin) were used to observe the microstructure and nanostructure. The crystal phase was investigated by powder X-ray diffraction (XRD) analysis (PANalytical, Empyrean, Cu Kα; λ = 0.1541 nm). X-ray photoelectron spectroscopy (XPS, Thermo Scientific, Escalab 250Xi, Al Kα at 1486.6 eV) and energy dispersive X-ray (EDS, Oxford, Xplore80) microanalysis were used to test the chemical composition and elemental distribution. The true content of Cu is measured by flame atomic absorption spectrophotometer (AAS, Beijing Purkinje General Instrument Co., Ltd., TAS-990). The materials were further measured by the specific surface area & pore size analyzer (Beishide Instrument, BSD-PS2). The materials were further characterized using photoluminescence (PL) emission spectroscopy (Edinburgh, FLS1000), UV−Vis diffuse reflectance spectroscopy (DRS, Shimadzu, UV-3600i Plus), and Fourier transform-infrared spectroscopy (FT-IR, Bruker, VERTEX 70). The CHI760E electrochemical workstation containing a three-electrode test system was used to measure electrochemical impedance spectroscopy (EIS) and photocurrent response data (more information referred to Supporting Information). Inductively coupled plasma emission spectrometry (ICP-OES, Thermo Scientific, iCAP 7000 Series) was used to quantify Cu$^{2+}$ leaching from the prepared materials in varied experimental conditions.

### 2.5. Disinfection tests

*P. aeruginosa* were selected as the model bacteria for sterilization test. The frozen stock of *P. aeruginosa* were seeded on a TSA plate and incubated at 37 °C for 24 h in an incubator oven (ZHICHENG, ZXDP-B2050). Subsequently, single colony of *P. aeruginosa* was inoculated into 20 mL TSB and cultivated in a shaking incubator (120 rpm, Honour, HNY-

**Fig. 1.** (a) Illustrative procedure for synthesis of hierarchical structure CuNPs/ZnIn$_2$S$_4$ (Cu/ZIS) nanocomposites. (b, c) TEM and (d) HRTEM images of 1.0 wt% Cu/ZIS nanocomposites. (e) The corresponding EDX elemental distribution mapping of Zn, In, S, and Cu within 1.0 wt% Cu/ZIS.

200B) at 37 °C for 18 h. Through centrifuging and washed with phosphate-buffered saline (PBS, 0.01 M, pH 7.4) solution, the harvested bacterial cells were resuspended in PBS with a cell density at $10^8$ colony forming units per mL (CFU mL$^{-1}$).

Influence factors involving level of irradiation (dark/light), dosage of ZIS (0–0.5 mg L$^{-1}$) and material types (*e.g.*, ZIS, 1.0 wt% Cu/ZIS) on disinfection were explored. Uniformly, 20 mL PBS suspension containing *P. aeruginosa* ($\sim 10^6$ CFU mL$^{-1}$) was stirred in the absence or presence of materials (0.1 g L$^{-1}$) and kept at room temperature *via* water circulation. 1 mL of the *P. aeruginosa* solution at each indicated time interval was aspirated and diluted in PBS solution. After appropriate dilution, 0.1 mL of the diluted sample was spread on agar plate followed by incubation at 37 °C for 24 h. Colonies were counted to determine the amount of viable bacteria. After disinfection, the solution of *P. aeruginosa* kept at room temperature in the dark. The density of bacteria was measured to monitor the bacterial regrowth within 24–48 h, respectively. In addition, the reusability of the materials was studied through five cycles of experiments. The practical application efficiency was also evaluated directly through disinfection of mix bacteria in natural water with initial concentration of $\sim 10^{3-4}$ CFU mL$^{-1}$, which was collected in Dongtiaoxi River (a tributary of Taihu Lake) at Zhejiang province. The experiment was repeated at least three times. All experiments were carried out in clean workbench (AIRTECH, SW-CJ-1FD). The consumables used in the experiments were sterilized in an autoclave (STIK CO. LTD, IMJ-85A) at 121 °C for 20 min or under ultraviolet radiation (254 nm) for 20–30 min

### 2.6. Leakage and decomposition of cell

The K$^+$ leaching after different disinfection times was quantified individually by using inductively coupled plasma emission spectrometry (ICP-OES, Agilent 720ES). The bacterial protein release with disinfection in progress was monitored and semi-quantified by a microplate reader (Thermo Fisher Scientific, Multiskan Sky). Live/Dead BacLight Bacterial Viability Kit (L7012, Molecular Probes) is a two-color fluorescence assay that was also conducted. The Live/Dead assay can be a reliable and qualitative approach to evaluate the integrity of the bacterial cell membranes (details are in Supporting Information) [12]. The fluorescence staining of bacteria was observed by fluorescence microscope (Olympus, BX43). The organic matter in solution during disinfection was analyzed by three-dimensional excitation-emission matrix fluorescence spectra (3D EEMs, Hitachi, F-4600).
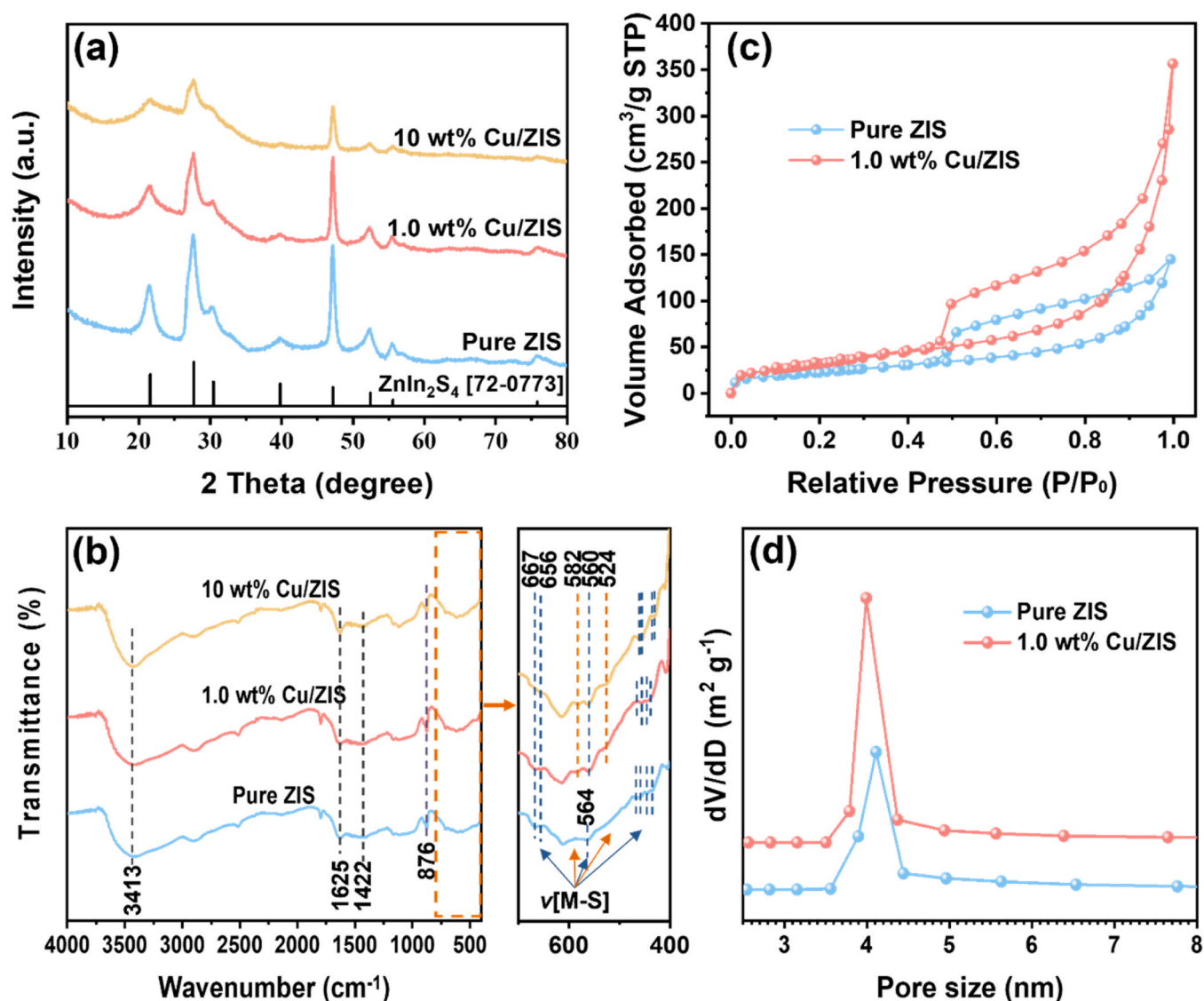
**Fig. 2.** (a) XRD patterns of pure ZIS, 1.0 wt% Cu/ZIS, and 10 wt% Cu/ZIS. (b) FT-IR transmittance spectra of pure ZIS, 1.0 wt% Cu/ZIS, and 10 wt% Cu/ZIS in the 400–4000 cm$^{-1}$. (c) Adsorption–desorption curves and (d) pore size distribution of the pure ZIS compared with 1.0 wt% Cu/ZIS.

### 2.7. Reactive species analyses

Electron paramagnetic resonance spectra (EPR, Bruker Elexsys E500-T) was used to verify HO$^{\bullet}$ and O$_2^{\bullet-}$ by spin-trapper DMPO. Moreover, 0.5 mM IPA and 2 mM TEMPO were served as scavengers for indicating the domination between HO$^{\bullet}$ and O$_2^{\bullet-}$, respectively.

## 3. Results and discussion

### 3.1. Synthesis and characterization

As show in Fig. 1a, synthesis evolution of hierarchical structure Cu/ZIS composite at mild conditions includes (1) facile hydrothermal synthesis of ZIS followed by (2) *in-situ* of CuNPs deposition on the surface of ZIS *via* photochemical deposition.

The morphology and nanostructure of Cu/ZnIn$_2$S$_4$ (denoted as Cu/ZIS) composites were systemically characterized *via* SEM and TEM. As the major component, the pure ZIS with a flower-like hierarchical architectures is constituted of multiple ultrathin nanosheets (Fig. S1a). On the other hand, the pure Cu nanoparticles directly prepared by photochemical deposition method are agglomerated (Fig. S1b). The

morphology of Cu/ZIS composites (Fig. S1c) is consistent with the pure ZIS's, but on the surface of the ZIS layers the CuNPs have been grown homogeneously through a photochemical deposition process in the visible wavelength range of 420–630 nm. As shown in TEM and HRTEM images of the as-prepared 1.0 wt% Cu/ZIS samples (Fig. 1b-d), the obtained results showed that Cu nanoparticles with diameters of < 10 nm are anchored on the surface of ZIS sheets. Moreover, with the increase of Cu loading, the size of Cu nanoparticles with agglomeration gradually became larger (Fig. S2a-d). The HRTEM images showed clearly that the D-spacing of the lattice fringes is 0.32 nm and 0.29 nm corresponding to the (102) and (104) planes of ZIS, respectively. The D-spacing of 0.20 nm is ascribed to the (111) plane of Cu [30,31]. Furthermore, in the as-prepared 1.0 wt% Cu/ZIS, the corresponding EDS elemental distribution mappings (Fig. 1e) shows that Cu has been implanted uniformly on ZIS by adopting the *in-situ* photochemical deposition method. These evidences reveal preliminarily that the self-assembled ZIS sheets with hierarchical structure could be used as a support for pseudo-homogeneously anchoring of the nano-scale copper particles (CuNPs, the size is less than 10 nm) by an *in-situ* photodeposition method.

The crystalline phases of the as-prepared samples were evaluated *via*

**Table 1**

A summary of surface area and pore structure for the as-prepared CuNPs, ZIS, 1.0 wt% Cu/ZIS samples.

| Catalysts | Surface area ($m^2\,g^{-1}$) | Total pore volume ($cm^3\,g^{-1}$) | Average pore diameter (nm) |
|---|---|---|---|
| ZIS | 83.8 | 0.22 | 10.4 |
| 1.0 wt% Cu/ZIS | 123.2 | 0.45 | 14.5 |
| Aggregated CuNPs | 39.1 | 0.25 | 25.7 |

XRD. As shown in Fig. 2a, the diffraction patterns of the samples (*i.e.*, 1.0 wt% Cu/ZIS and 10 wt% Cu/ZIS) are consistent with that of pure ZIS (ZnIn$_2$S$_4$, JCPDS No. 72–0773) [32,33]. Nevertheless, the decoration of Cu with the increase of mass ratio could lead to a decline in the intensity of the ZIS characteristic diffraction peaks in Cu/ZIS composites. Meanwhile, the peak widths of Cu/ZIS become slightly wider as compared with those of the pristine ZIS [34]. Although the characteristic peaks of specific crystal forms of CuNPs cannot be observed in the pattern of Cu/ZIS, it is reasonable to realize the presence of CuNPs in the as-prepared composite because the intensity of ZIS characteristic peaks is becoming weak with the increase in Cu loading [35,36]. In the FT-IR transmittance spectra (Fig. 2b), the strong peak at 3413 cm$^{-1}$ is attributed to the O−H bond stretching vibrational modes of adsorbed H$_2$O moisture in the as-prepared samples [37]. It is obvious that the intensity exhibited stronger with the loading Cu in the composites. The water molecules adsorption enhancement is possibly ascribed the surface property change (Cu decorated) and the enhancement of surface area (Table 1). The peaks at 1625 cm$^{-1}$ and 1422 cm$^{-1}$ are probably assigned to the bending vibration of hydroxyl groups on the surface of nano-materials [38]. In the samples, the vibrational modes of sulfur− [transition metal ions] ($v$(M−S)) detected are very similar to ZIS in the 400–900 cm$^{-1}$ region [39,40]. It is worth noticing that characteristic peaks appeared at 582 cm$^{-1}$ and 524 cm$^{-1}$ in Cu/ZIS compared to ZIS, which may be attributed to the decorated CuNPs [41–43]. The peaks of ZIS in the 665, 564, and 468–435 cm$^{-1}$ region are slightly shifted due to the CuNPs interaction [12], suggesting that Cu/ZIS composite has been successful in building up of internal CuNP-ZIS interaction. Furthermore, the composition of the obtained Cu/ZIS samples was determined by AAS (Fig. S3). The mass percentages of metallic Cu measured in x wt% Cu/ZIS samples (x = 0.5, 1.0, 2.0, 10) are about 0.34%, 0.92%, 1.71%, and 9.98%, respectively, which are close to the experimental designed ratio.

The N$_2$ adsorption-desorption experiment was utilized to grasp the specific surface area and pore size distribution for the as-prepared representative samples (Fig. 2c). Apparently, all samples have representative IV adsorption isotherms with H3 hysteresis loop, which imply the features of mesoporous structure. Fig. 2d shows the pore size distributions of pure ZIS and 1.0 wt% Cu/ZIS samples calculated from analytical data using the Barrett-Joyner-Halenda (BJH) model, mainly in the range of 3.5–4.5 nm with mesoporous features. As shown in Table 1, the BET surface area of CuNPs, ZIS, and 1.0 wt% Cu/ZIS are 39.1, 83.8, and 123.2 m$^2$ g$^{-1}$, respectively. The specific surface area and pore volume of the Cu/ZIS nanocomposites increase with the
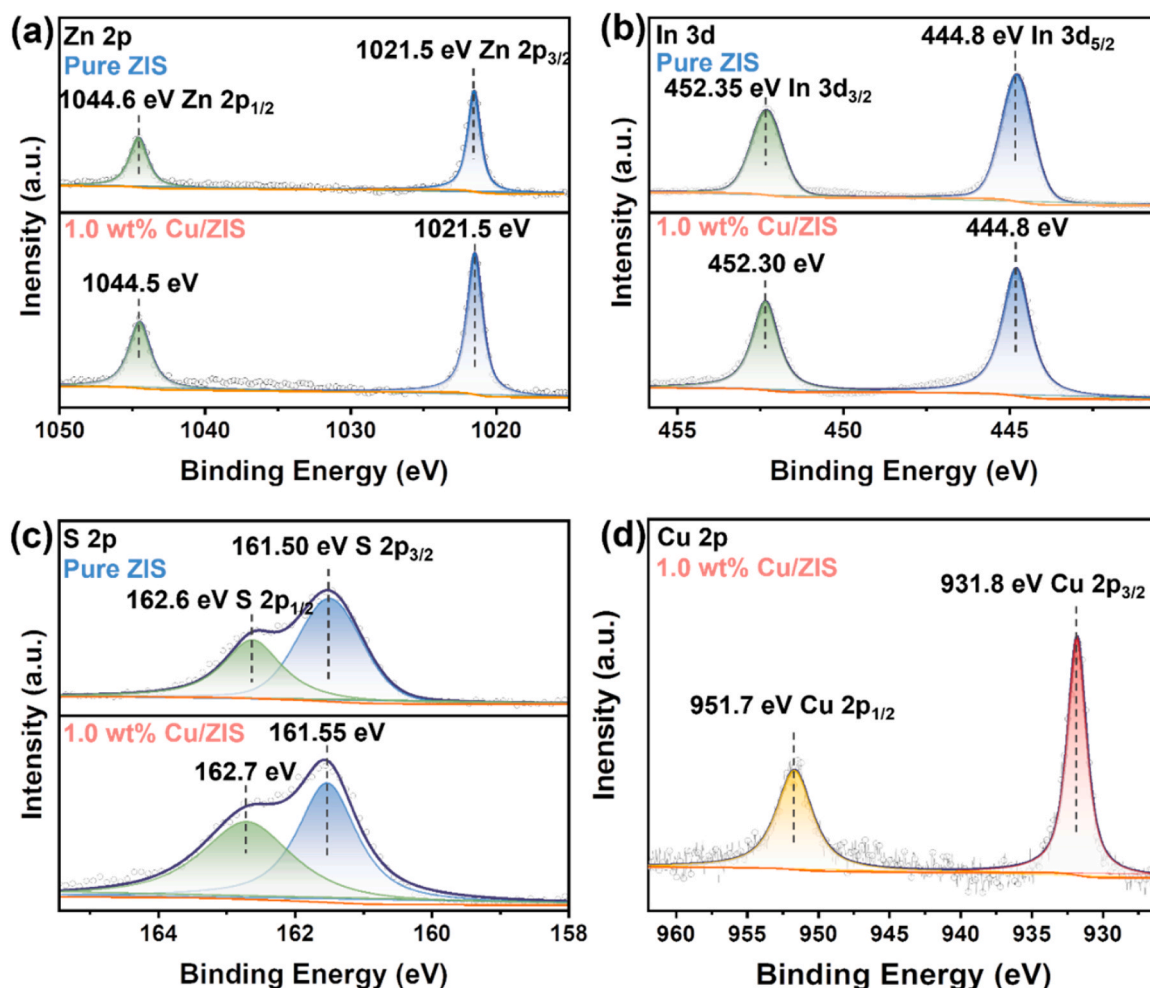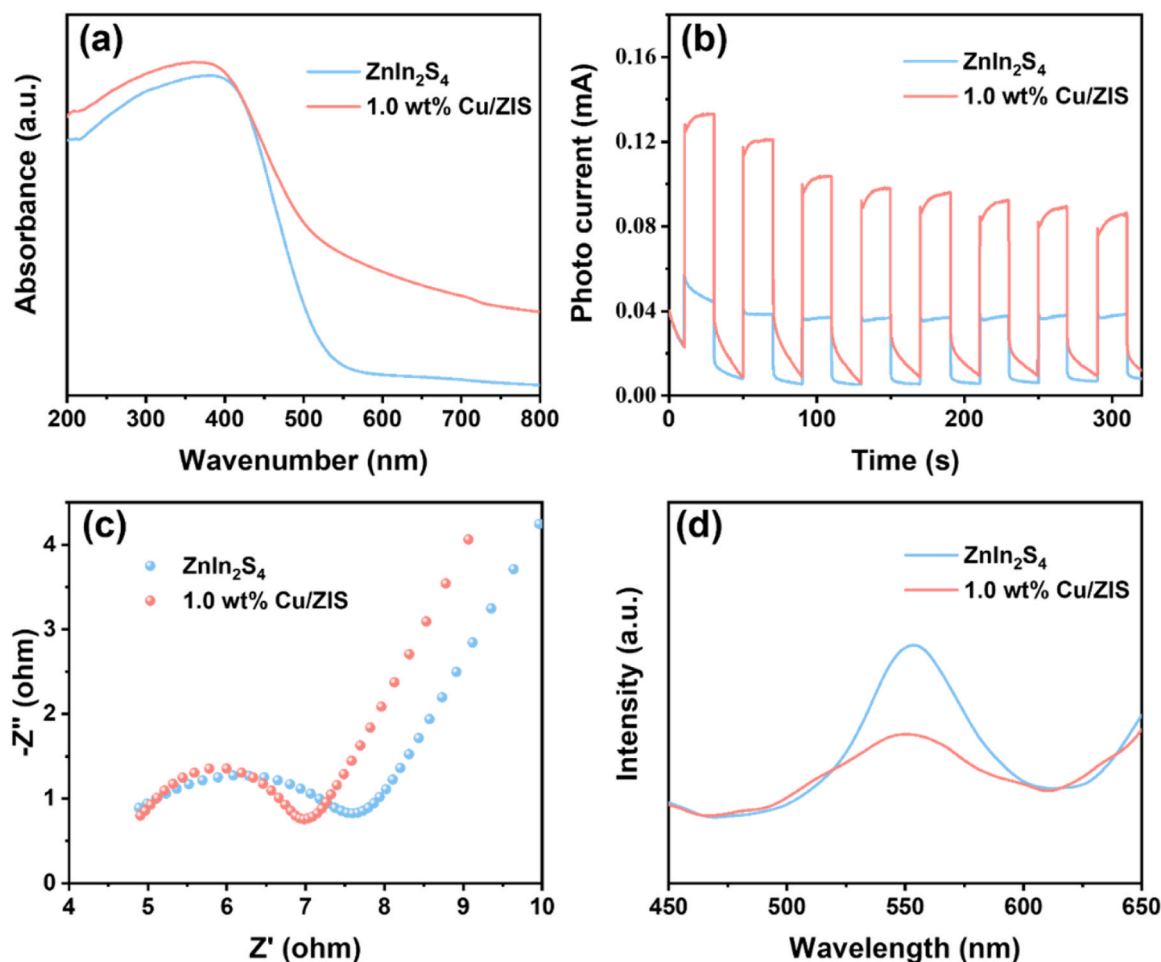


**Fig. 3.** (a) Typical Zn 2p, (b) In 3d, and (c) S 2p XPS spectra of pure ZIS, 1.0 wt% Cu/ZIS. (d) typical Cu 2p XPS spectrum of 1.0 wt% Cu/ZIS.

**Fig. 4.** (a) UV–vis absorption spectra, (b) transient photocurrent responses, (c) electro- chemical impedance spectroscopy plots and (d) photoluminescence spectra of $ZnIn_2S_4$ and 1.0 wt% Cu/ZIS samples.

introduction of CuNPs. It may be attributed to the highly dispersed CuNPs cooperating with ZIS nanosheet petals, which resulted in the change of ZIS surface structure with increasing roughness [44]. However, the excessive Cu nanoparticles decorated on the surface of ZIS that will lead to the decrease of the specific surface area of the composites (Table S1), which is possible attributed to the effect of agglomeration and pore blockage. Overall, the achieved CuNP-decorated ZIS with specific surface structure is possibly beneficial to improve the interaction between disinfectants with microorganisms. Meanwhile, it also can enhance the rate of interface charge transfer during the photocatalytic process with postponing/reducing photogenerated carrier recombination.
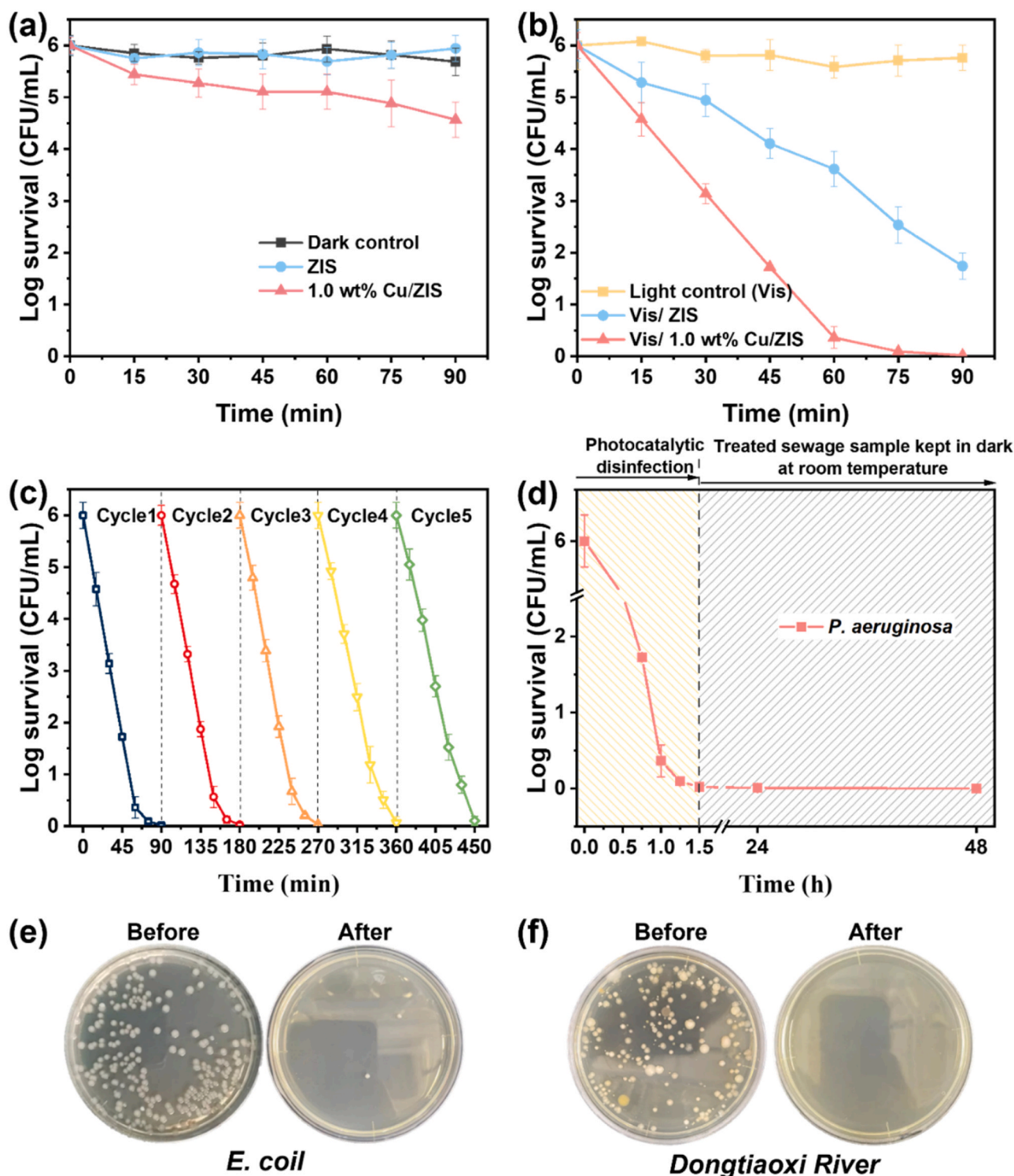
Moreover, XPS was used for the as-prepared samples to study the chemical states of different elements. Regarding the XPS survey spectra (Fig. S4a), the spectra contain not only Cu 2p from decorated materials, but also Zn 2p, In 3d, and S 2p from supporting materials, which further confirms that the CuNPs have been successfully anchored on the ZIS [34]. Fig. 3a shows the two peaks in Zn 2p monitored to $Zn^{2+}$ are observed at 1044.6 eV (Zn $2p_{1/2}$) and 1021.5 eV (Zn $2p_{3/2}$), clearly [45]. In addition, the peaks of In 3d at 452.35 eV (In $3d_{3/2}$) and 444.8 eV (In $3d_{5/2}$) as well as S 2p at 162.6 eV (S $2p_{1/2}$) and 161.5 eV (S $2p_{3/2}$) can be assigned to $In^{3+}$ and $S^{2-}$ of the pristine ZIS (Fig. 3b-c), respectively [29]. As shown in Fig. 3d, the characteristic binding energies of Cu 2p3/2 and Cu 2p1/2 at 931.8 and 951.7 eV can be detected in 1.0 wt% Cu/ZIS but without satellite peaks of $Cu^{2+}$ existing, which initially indicates that Cu in the composites mainly present in the $Cu^0$ and $Cu^+$ states (the further demonstration of $Cu^0/Cu^+$ by Auger electron spectroscopy (AES) as

shown in Fig. S5) [46]. Meanwhile, the peaks of Zn 2p, In 3d, and S 2p made a light shifting in 1.0 wt% Cu/ZIS, indicating a strong electronic interactions formed between Cu and ZIS, rather than a simple mixture [27,47]. These results further confirm that ZIS surfaces modified with CuNPs can be achieved through a simple room temperature photochemical deposition reaction.

### 3.2. Photoelectrochemical measurements

UV–vis diffuse reflectance spectrum (Fig. 4a) displays the light harvesting capability of pure ZIS and 1.0 wt% Cu/ZIS. It can be observed that ZIS has a good performance in light absorption in visible light region below 550 nm (see blue curve). While the light harvesting behavior of 1.0 wt% Cu/ZIS samples are significantly becoming higher and broad with loading CuNPs (see red curve), indicating that the deposition of Cu can comprehensively improve the light absorption capacity of ZIS photocatalysts [47]. Meanwhile, the band energy ($E_g$) of the samples can be estimated according to the Tauc plot. As shown in Figs. S4b and S6a-b, the $E_g$ of the as-prepared samples shift slightly from 2.52 to 2.49 eV after decorated CuNPs was obtained with the valence band potential at 1.23 eV.

To further investigate the influence of Cu decoration on separation and transportation efficiency of photogenerated carriers within ZIS, the photocurrent responses of pure ZIS compared with 1.0 wt% Cu/ZIS samples were measured [48]. The results in Fig. 4b showed that Cu/ZIS has a higher photogenerated electron transfer rate, implying that the photogenerated carriers in ZIS would be easier to separate and transport

**Fig. 5.** Comparison of the disinfection efficacies of ZIS and 1.0 wt% Cu/ZIS *via* contact with *P. aeruginosa* cells in dark (a) and in visible light irradiation (b), respectively (Experimental conditions : catalyst load = 0.1 g L$^{-1}$, exposure time = 90 min, pH= ~7.4, initial concentration = 10$^6$ CFU mL$^{-1}$). (c) Reproducibility performance of 1.0 wt% Cu/ZIS disinfectant towards *P. aeruginosa*. (d) Bacteria regrowth test *P. aeruginosa* cells after Vis/Cu/ZIS disinfection. Colony number of (e) *E. coil* and (f) mix bacteria in natural water (collected in the Dongtiaoxi River) before and after disinfection.

by the decorated Cu with a predictably better catalytic activity. On the other hand, electrochemical impedance spectroscopy (EIS) is another way to examine the photogenerated charge transfer ability in Cu/ZIS samples compared with the pristine ZIS [49]. From the data in Fig. 4c, it can be seen that the semicircle of Cu/ZIS is smaller than that of pure ZIS, which further indicates that Cu loading indeed improves the charge

transfer ability within Cu/ZIS composites. PL emission spectroscopy is commonly used to study the excited states of electrons in the micro-structures of materials [50]. This technique probably reflects the be-haviors on carriers capture and recombination in semiconductors. As shown in Fig. 4d, it is worth noting that the fluorescence peak intensity of Cu/ZIS is lower than that of ZIS, which means that the loading of Cu

**Table 2**
$Cu^{2+}$ released when the synthesized samples used in disinfection system.

| Time (h) | $Cu^{2+}$ released ($\mu g\ L^{-1}$)[a] | | |
|---|---|---|---|
| | Dark/1.0 wt% Cu/ZIS | Vis/1.0 wt% Cu/ZIS | Vis/CuNPs |
| 0 | - | - | - |
| 1.5 | 131.5 | 26.7 | 256.6 |
| 12 | 322.7 | 67.5 | 389.9 |
| 24 | 310.7 | 101.6 | 469.2 |

[a] $Cu^{2+}$ leaching measurement using ICP-OES

effectively reduces the recombination rate of photoelectrons and holes ($e^-/h^+$) in the material [51]. This result corroborates the photocurrent response and EIS analysis results.
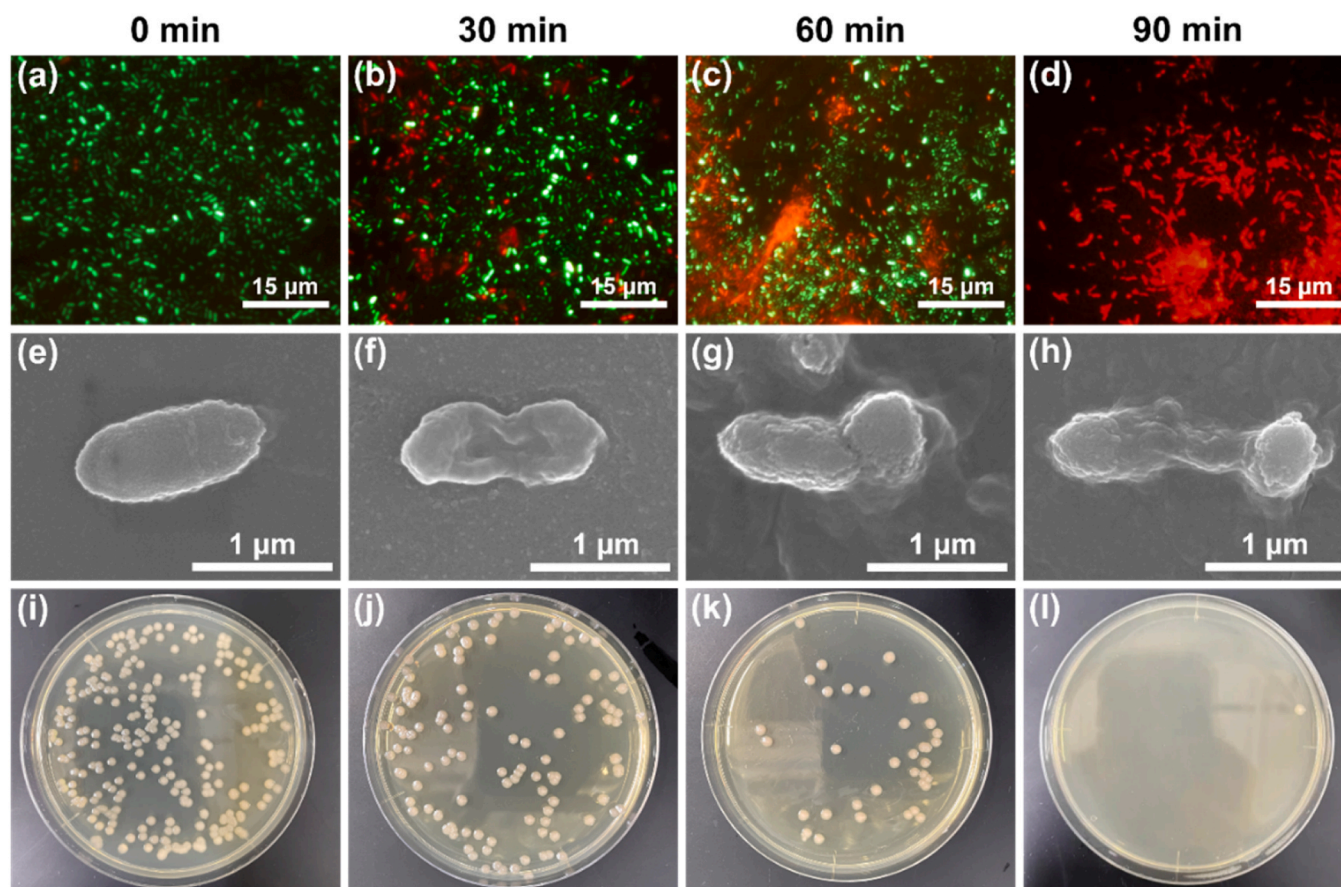
## 3.3. Disinfection performance

As shown in Fig. 5a, the antibacterial properties of varied materials were evaluated by the model bacteria of *P. aeruginosa* in the dark. ZIS did not deactivate bacteria while the viability of *P. aeruginosa* remains intact in the dark at controlled experimental conditions (Fig. 5a), indicating that ZIS is nontoxic to bacteria at a dosage of 0.1 g $L^{-1}$. It is obvious that 1.0 wt% Cu/ZIS with loaded CuNPs performed a higher bactericidal performance than ZIS, which is attributed to the antibacterial property of CuNPs [16]. This is confirmed by the significantly higher disinfection efficiency of the *P. aeruginosa* of the as-prepared pure Cu as compared to that of pure ZIS (Fig. S7). The penetration of the released CuNPs into the cells may result in the interruption of intracellular metabolic pathways (*e.g.*, suppressing adenosine triphosphate formation and enzymes activity), as well as its physical damage of cell membrane through direct

contact of the interface of Cu/ZIS with bacterial cells [17,18].

Fig. 5b illustrates the cell survival status of *P. aeruginosa* in photocatalytic system in the presence of ZIS or Cu/ZIS composites. The material dosage was optimized at 0.1 g $L^{-1}$ (Fig. S8). After being irradiated by visible light at wavelength of 420–630 nm, the antibacterial properties for Cu-decorated ZIS are significantly higher than that of ZIS. The corresponding cell survival of *P. aeruginosa* declined to 1.74 logs and 0.01 logs after co-cultivation with ZIS or 1.0 wt% Cu/ZIS for 90 min, respectively. Apparently, 1.0 wt% Cu/ZIS shows remarkable bactericidal performance of approaching 100% in Vis/disinfectant system. Varied loadings of CuNPs in Cu/ZIS composite were used for testing disinfection efficacies as well (Fig. S9). The results indicated that an appropriate ratio of Cu/ZIS is beneficial for balancing the interaction between Cu and ZIS components, which makes the nanocomposites show an optimal bactericidal performance. As shown in Table 2, the Cu run off is seriously increasing to levels above hundreds ppb (part per million) with the increase reaction time both in dark/1.0 wt% Cu/ZIS system or Vis/CuNPs system (the Cu dosage used in disinfection system equals to 1.0 wt% Cu in Cu/ZIS composites). However, in Vis/1.0 wt% Cu/ZIS system, the Cu release obviously become less and stabilizes at a level of 67.5 $\mu g\ L^{-1}$ after 12 h. It is worth noting that the released Cu in functioning as a disinfectant probably regenerated at the same time through cooperating with ZIS-driven photocatalysis. This means that a few of photogenerated electrons are possibly used for reduction of the charged Cu atoms *in-situ* on the surface of ZIS [48]. In this kind of synergistic system at nano/micro-scale, the Cu/ZIS composites in visible light irradiation show the best sterilization effect rather than that of Cu and ZIS (Fig. S10, Fig. 5b) while simultaneously ensuring the sustainability of its lifespan (Table 2).

As shown by the log reduction values within five cycles of



**Fig. 6.** (a-d) Fluorescence images (recorded using dual color channels), (e-f) SEM images, and (i-l) colony number in agar plate of *P. aeruginosa* recording dynamically in Vis/Cu/ZIS disinfection process.
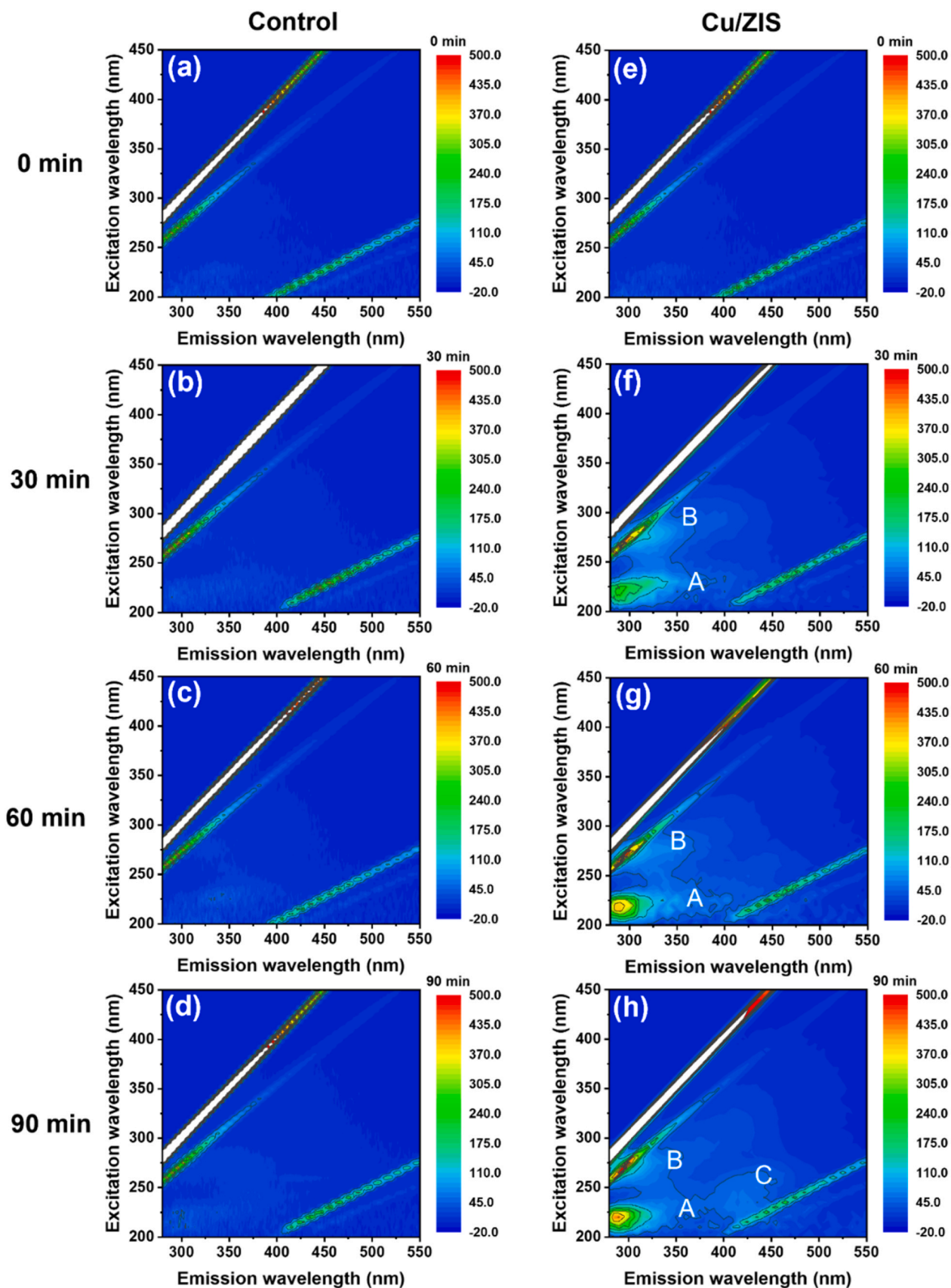
**Fig. 7.** 3D EEMs dynamically recording the release of intracellular organic maters in the absence of Cu/ZIS disinfectant (a-d) and in the presence of Cu/ZIS disinfectant (e-h).
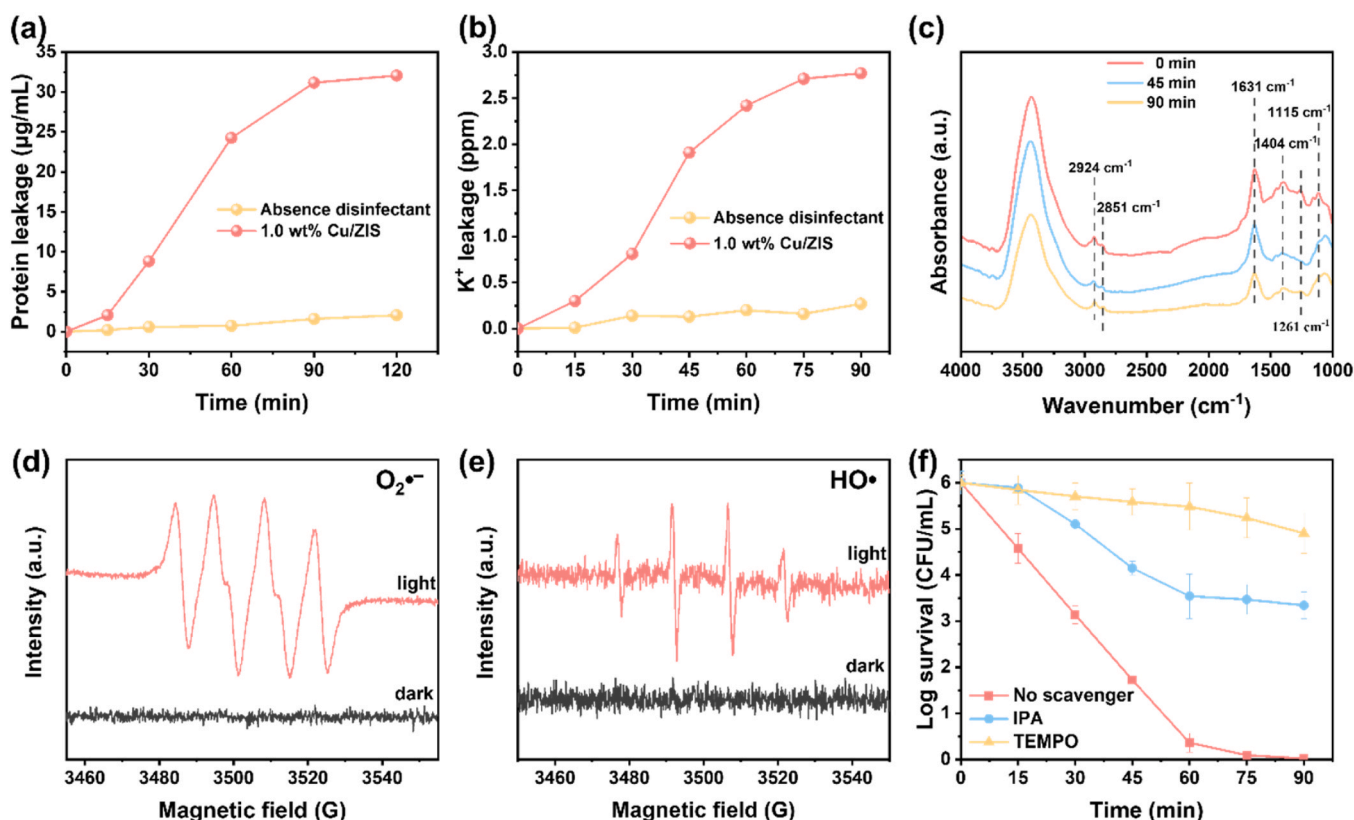
**Fig. 8.** (a) Protein leakage, (b) $K^+$ leakage, and (c) FT-IR spectra vibration during the disinfection process of *P. aeruginosa*. EPR spectra upon for detection of (d) $O_2^{\bullet-}$, (e) $HO^\bullet$ in Vis/Cu/ZIS system. (f) Effect of varied radical capture agents on the disinfection efficacies in Vis/Cu/ZIS system.

antibacterial experiments (Fig. 5c), the disinfection performance of 1.0 wt% Cu/ZIS maintained a good stable performance, which can be attributed to the effective suppression of the loss of CuNPs decorated on ZIS. Comparing the SEM images before and after 5 cycles, the hierarchical structure of ZIS (Fig. S11) appear to be well-preserved while the crystal structure (Fig. S12) also did not change. After disinfection under controlled experimental conditions in visible light irradiation, a bacterial regrowth testing was carried out (Fig. 5d). The phenomenon indicates that the deactivated bacterial cells in Vis/Cu/ZIS system cannot be revived in 48 h, which reflects that the disinfection might cause irreversible damage [52]. Besides *P. aeruginosa*, the Vis/Cu/ZIS system was also effective in deactivating *E. coil* (Fig. 5e) in another model bacteria and mixed bacteria in natural water (*i.e.*, actual water sample collected in Dongtiaoxi River) (Fig. 5 f). In summary, 1.0 wt% CuNPs/ZnIn$_2$S$_4$ has good cyclic sterilization ability, stability and disinfection effects, as well as providing good potential for its practical application in natural water.
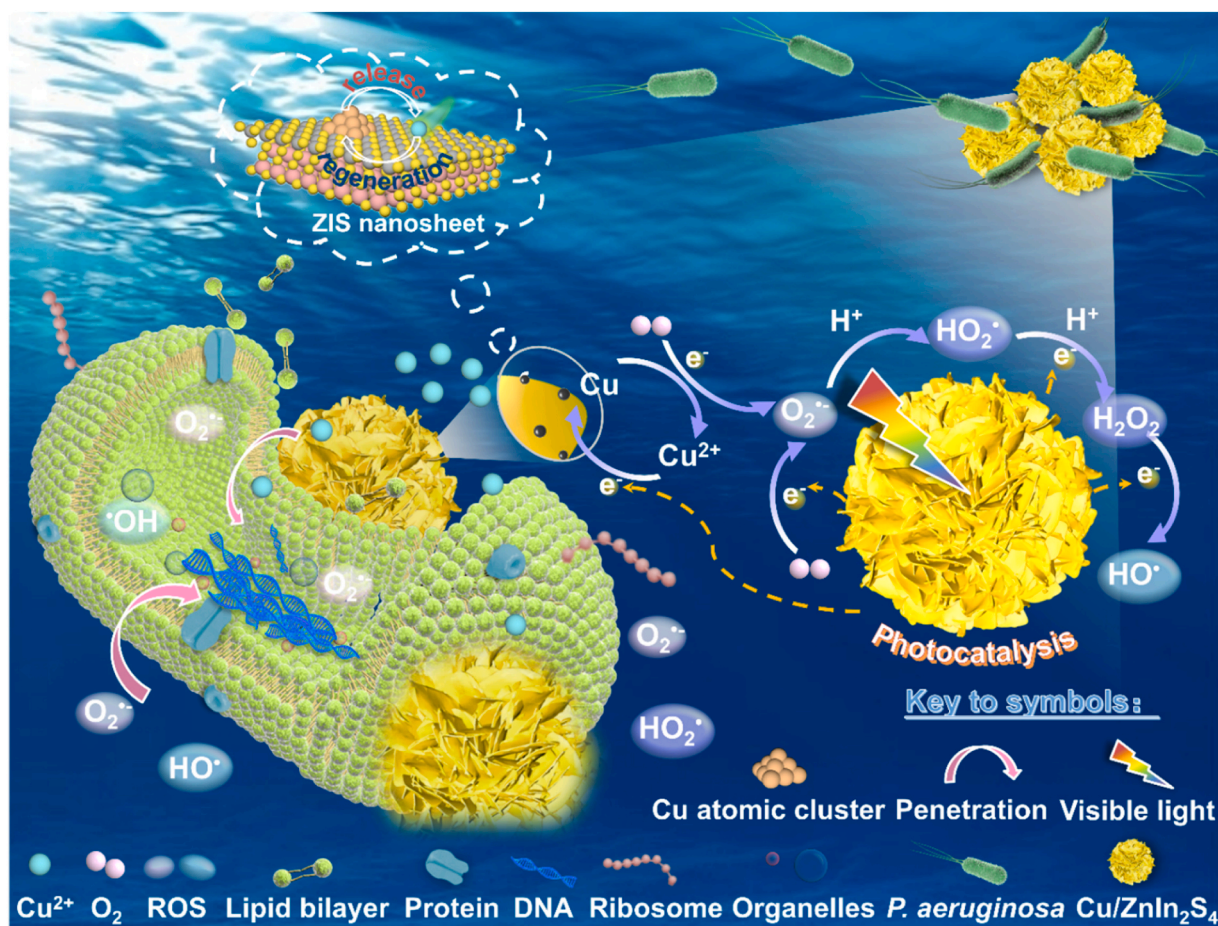
### 3.4. Mechanism of Cu/ZIS's bacterial inactivation

The variation of bacterial status and cell membrane integrity of *P. aeruginosa* during the disinfection process were quasi-dynamically visual-observed by fluorescence microscopy (Fig. 6a-d), SEM (Fig. 6e-h), and agar plate count (Fig. 6i-l) [53]. At the beginning of the disinfection stage in presence of 1.0 wt% Cu/ZIS under visible light, all of the living bacteria are stained green (Fig. 6a) and appear as intact rods (Fig. 6e). The agar plate count shows the survival of bacterial colonies copiously (Fig. 6i). After 30 min, a few bacterial cells are stained red (Fig. 6b), indicating that the integrity of the cell membrane was damaged. With the extension of reaction time, the red parts replaced the green ones gradually (Fig. 6c) along with cells becoming distorted and their membrane edges blurred (Fig. 6 g), indicating that the most cells

have lost their membrane integrity in this Vis/Cu/ZIS disinfection system [54]. After 90 min, all of the bacterial cells are stained red (Fig. 6d) associated with the fold and fracture of membranes (Fig. 6 h), suggesting that the bacterial cells have been destroyed at both the intracellular and extracellular tissue level [55]. That is a probable reason why the deactivated bacteria based on Cu/ZIS disinfectants cannot be revived (Fig. 5d). The observed colonies gradually fade away (Fig. 6j-l).

As shown in Figs. 7, 3D EEM spectra was used to quasi-dynamically illustrate the intracellular organic maters release when the cell membranes suffered from damage in the Vis/Cu/ZIS disinfection system. As a comparison, there are no specific changes of fluorescence peaks on the extracellular organic maters during *P. aeruginosa* growth process in visible light irradiation (Fig. 7a-d). There is also no obvious signal vibration at the beginning in Cu/ZIS driven disinfection system under visible light irradiation (Fig. 7e). With the damage of cell membranes and death of bacteria, the fluorescence peaks denoted as A and B were detected and becoming strong gradually (Fig. 7f-h): A at Ex/Em was 220 nm/285 nm, B at Ex/Em was 270/295 nm. They are attributed to aromatic protein-like and tryptophan proteins-like along with intracellular organic matter released from the destruction of the cells during the Cu/ZIS disinfection process [56]. With the further extension of time to 90 min (Fig. 7 h), additional peak C detected at Ex/Em of 220 nm/420 nm was identified as fulvic acid-like compounds. It is plausible that the intracellular substances were decomposed and further transformed into small molecule compounds, such as fulvic acid-like and humic acid-like compounds (Fig. S13), when attacked by the *in-situ* generated reactive oxygen species (ROSs) [57].

The released intracellular organic matters including protein and $K^+$ ions were verified and quantified subsequently. As shown in Fig. 8a and b, the amount of protein and $K^+$ leaked in Vis/Cu/ZIS disinfection system is significantly higher than that in the absence of disinfectants. With the cell membrane damage, the intracellular concentration in bulk

**Fig. 9.** Illustration displaying the proposed bactericidal mechanism based on Cu/ZIS disinfectants by functioning as CuNPs *in-situ* regeneration and ZIS visible-light photocatalysis.

solution is increasing steadily and gradually. In addition, the leakage was characterized by FT-IR spectra (Fig. 8c). The characteristic peaks at 1115, 1261, 1404, 1631, 2851 and 2924 $cm^{-1}$ are probably ascribed to the organic matters such as amide II, phospholipid phosphate dibasic, polysaccharide sugar ring and other groups shown in Table S2 [58,59].

As mentioned previously, the ROSs played a key role in cell membranes damage in this study. Through the as-prepared 1.0 wt% Cu/ZIS composites, the as-formed ROSs were identified by ESR using DMPO as spin traps. The strong characteristic peaks referring to $O_2^{\bullet-}$ (Fig. 8d) and $HO^{\bullet}$ (Fig. 8e) were estimated under visible light irradiation. Moreover, IPA and TEMPO as radical scavengers were individually used to quench $HO^{\bullet}$ and $O_2^{\bullet-}$ in Cu/ZIS driven disinfection system. The results shown in Fig. 8f had indicated that $O_2^{\bullet-}$ is the dominant ROSs for destroying cell membranes followed by $HO^{\bullet}$. Therefore, we propose a plausible ROS transformation pathway within Cu/ZIS based on a bandgap of 2.49 eV (Fig. S14). Cu/ZIS generated $e^-/h^+$ pairs upon photocatalysis have the valence band (VB) and conduction band (CB) potential of 1.23 V and $-1.26$ V (Figs. S4b and S6b), respectively. As compared in Table S3, the VB of Cu/ZIS is lower than $E^{\theta}$ ($HO^{\bullet}/H_2O$) and $E^{\theta}$ ($HO^{\bullet}/HO^-$), indicating that the generated $h^+$ is not enough to oxidize $H_2O$ or $OH^-$ to generate $HO^{\bullet}$, but can be successful for conversion $H_2O$ into $O_2$ ($E^{\theta}$ ($H_2O/O_2$) $= 1.229$ V *vs* SHE) [29]. As shown in Fig. S14, both the autogenerated and dissolved $O_2$ can be converted into $O_2^{\bullet-}$ and other ROSs through reacting with $e^-$.

Based on above results achieved in this study, a plausible bactericidal mechanism in Cu/ZIS disinfection system is proposed (Fig. 9). The decorated CuNPs on the surface of ZIS can be released through conversion of Cu atomic clusters into $Cu^{2+}$ ions (Fig. 9, see ZIS nanosheet) in

light irradiation (an operando EPR experiment as an evidence shown in Fig. S15) [60]. After that the penetrated $Cu^{2+}$ can interrupt the intracellular metabolic pathways of the bacteria [16]. The free-diffusing $Cu^{2+}$ on the interface of ZIS will be regenerated by using photogenerated electrons (Fig. 9 see Photocatalysis). That is why Cu release become lower in Vis/Cu/ZIS disinfection system than the others (Table 2). As evidenced from EPR results (Fig. S16), in spite of the remarkable enhanced separation of photogenerated carriers in Cu/ZIS photocatalysis system (Fig. 4), the EPR signal for radical formation in Cu/ZIS photocatalysis does not become stronger compared with that of pure ZIS. This phenomenon further consolidates that the enhanced bactericidal in Vis/Cu/ZIS system is not only originated from the promoted ROS generation, whereas the special $Cu^{2+}$-releasing mechanism in Cu/ZIS should be responsible. In the meanwhile, when considering the gap between the enhanced photo-generated carriers in Cu/ZIS and the almost identical ROS generation from photo-generated carriers between Cu/ZIS and Cu, it can be proposed that extra photogenerated carriers in Cu/ZIS should contribute to the *in-situ* regeneration $Cu^{2+}$ into $Cu^0/Cu^{1+}$.

Finally, it is worth noting that in Cu/ZIS, a hybrid bactericidal process is proceeded. Besides the release of $Cu^{2+}/Cu^+$, the abundant $e^-$ formed in Cu/ZIS-driven photocatalysis are also utilized for the production of ROSs (*i.e.*, $O_2^{\bullet-}$) (identified in Fig. 8d) because the valence band and conduction band of the as-prepared ZIS is located at 1.23 eV and $-1.26$ eV approximately (Figs. S4b, S6 and S14). The redox potential is only enough for transformation of $O_2/O_2^{\bullet-}$ rather than $H_2O/HO^{\bullet}$. Therefore, the other ROSs (*e.g.*, $HO^{\bullet}$) shown in Fig. 9 (photocatalysis based on Cu/ZIS) are generated in the way of species

transformation through consuming electrons. All of the ROSs can contribute to cell membranes damage, intracellular organic matters degradation, and lipid bilayer decomposition. In this well-designed Vis/Cu/ZIS disinfection system, the *P. aeruginosa* can be sterilized absolutely under internal and external attacks (Fig. 6). It results in leakage of intracellular substances (Figs. 7 and 8) culminating in irrevocable cell death (Fig. 5d).

## 4. Conclusions

In summary, we have successfully demonstrated the design and fabrication of a novel CuNPs/ZnIn$_2$S$_4$ (Cu/ZIS) disinfectant with pseudo-homogeneously decorating CuNPs ($< 10$ nm) on the surface structure of ZIS sheets by photodeposition at room temperature. Using the 3D EEM spectrometer, fluorescence microscopy, SEM, and agar plate simultaneously, the *P. aeruginosa* death process, which is cell membrane damage and intracellular compounds leakage (*e.g.*, K$^+$, protein-like, tryptophan-like, and fulvic acid-like) in the Vis/Cu/ZIS catalysis disinfection system has been quasi-dynamically visualized. Based on the evaluation tests referring to the as-prepared samples (*i.e.*, aggregated CuNPs, ZIS, and Cu/ZIS) both in the dark and in the visible-light irradiation, the Cu/ZIS-driven catalytic disinfection under 420–630 nm light irradiation exhibited the highest bactericidal efficiency of 100% (the initial is 10$^6$ CFU mL$^{-1}$) associated with hindering bacteria regrowth and suppressing Cu loss. Combining all of the achieved results, we propose a plausible bactericidal mechanism that was elucidated based on a novel concept proposed about *in-situ* regeneration of Cu atomic clusters by using photogenerated electrons, and significant promotion of the formation of ROSs (O$_2^{\bullet-}$, HO$^\bullet$) with postponing/reducing the recombination of photogenerated carriers. Compared with the Cu and ZIS components, the achieved Cu/ZIS disinfectant has a remarkable bactericidal performance with a long lifespan not only for model bacteria in artificially contaminated water but also for mixed bacteria in natural water (*e.g.*, Dongtiaoxi River, Zhejiang Province). It provides a facile method to design novel disinfectants with high efficiency, economy, safety, and long lifespan for enhancing the development of a neoteric sterilization technology (denoted as "catalytic disinfection"), and provide new insights into disinfection of harmful microorganism *via* exposure to indoor lighting.

## CRediT authorship contribution statement

**Zhong-Ting Hu**: Resources, Conceptualization, Writing – review & editing, Supervision, Project administration, Funding acquisition. **Yan-Fei Fei**: Methodology, Formal analysis, Investigation, Data curation, Writing – original draft, Visualization. **Qiong-Yu Wang**: Investigation, Methodology, Data curation. **Qi Zhao**: Formal analysis, Investigation, Data curation. **Siew-Leng Loo**: Investigation, Formal analysis. **Mian Hu**: Investigation, Data curation. **Yonghe Li**: Investigation, Formal analysis. **Yujie Song**: Investigation, Data curation. **Jie-Xin Wang**: Methodology, Data curation. **Zhi-Gang Shen**: Investigation, Data curation. **Hua Sheng**: Resources, Conceptualization, Writing – review & editing, Supervision, Project administration, Funding acquisition. **Jiade Wang**: Resources, Conceptualization, Writing – review & editing, Supervision, Project administration, Funding acquisition. **Jincai Zhao**: Supervision.

## Declaration of Competing Interest

The authors declare that they have no known competing financial interests or personal relationships that could have appeared to influence the work reported in this paper.

## Data availability

Data will be made available on request.

## Appendix A. Supporting information

Supplementary data associated with this article can be found in the online version at doi:10.1016/j.apcatb.2023.122995.

## References

[1] A. Saravanan, P.S. Kumar, S. Jeevanantham, S. Karishma, A.R. Kiruthika, Photocatalytic disinfection of micro-organisms: Mechanisms and applications, Environ. Technol. Innov. 24 (2021) 101909–101923, https://doi.org/10.1016/j.eti.2021.101909.

[2] J. Portelinha, S.S. Duay, S.I. Yu, K. Heilemann, M.D.J. Libardo, S.A. Juliano, J.L. Klassen, A.M. Angeles-Boza, Antimicrobial peptides and copper(II) ions: Novel therapeutic opportunities, Chem. Rev. 121 (2021) 2648–2712, https://doi.org/10.1021/acs.chemrev.0c00921.

[3] C. Zhang, Y. Li, D. Shuai, Y. Shen, D. Wang, Progress and challenges in photocatalytic disinfection of waterborne Viruses: A review to fill current knowledge gaps, Chem. Eng. J. 355 (2019) 399–415, https://doi.org/10.1016/j.cej.2018.08.158.

[4] L. Wang, Z. Hu, M. Hu, J. Zhao, P. Zhou, Y. Zhang, X. Zheng, Y. Zhang, Z.T. Hu, Z. Pan, Cometabolic biodegradation system employed subculturing photosynthetic bacteria: A new degradation pathway of 4-chlorophenol in hypersaline wastewater, Bioresour. Technol. 361 (2022) 127670–127678, https://doi.org/10.1016/j.biortech.2022.127670.

[5] Z.T. Hu, Y. Chen, Y.F. Fei, S.L. Loo, G. Chen, M. Hu, Y. Song, J. Zhao, Y. Zhang, J. Wang, An overview of nanomaterial-based novel disinfection technologies for harmful microorganisms: Mechanism, synthesis, devices and application, Sci. Total. Environ. 837 (2022) 155720–155740, https://doi.org/10.1016/j.scitotenv.2022.155720.

[6] G. Zhang, W. Li, S. Chen, W. Zhou, J. Chen, Problems of conventional disinfection and new sterilization methods for antibiotic resistance control, Chemosphere 254 (2020) 126831–126842, https://doi.org/10.1016/j.chemosphere.2020.126831.

[7] J. Lu, J. Guo, Disinfection spreads antimicrobial resistance, Science 371 (2021) 474, https://doi.org/10.1126/science.abg438.

[8] S. Zhang, Y. Wang, J. Lu, Z. Yu, H. Song, P.L. Bond, J. Guo, Chlorine disinfection facilitates natural transformation through ROS-mediated oxidative stress, ISME J. 15 (2021) 2969–2985, https://doi.org/10.1038/s41396-021-00980-4.

[9] Z.Y. Huo, Y. Du, Z. Chen, Y.H. Wu, H.Y. Hu, Evaluation and prospects of nanomaterial-enabled innovative processes and devices for water disinfection: A state-of-the-art review, Water Res. 173 (2020) 115581–115596, https://doi.org/10.1016/j.watres.2020.115581.

[10] W. Gao, L. Zhang, Nanomaterials arising amid antibiotic resistance, Nat. Rev. Microbiol. 19 (2021) 5–6, https://doi.org/10.1038/s41579-020-00469-5.

[11] J.M.V. Makabenta, A. Nabawy, C.H. Li, S. Schmidt-Malan, R. Patel, V.M. Rotello, Nanomaterial-based therapeutics for antibiotic-resistant bacterial infections, Nat. Rev. Microbiol. 19 (2021) 23–36, https://doi.org/10.1038/s41579-020-0420-1.

[12] Z.T. Hu, Y.N. Liang, J. Zhao, Y. Zhang, E.H. Yang, J. Chen, T.T. Lim, Ultra-effective integrated technologies for water disinfection with a novel 0D–2D-3D nanostructured rGO-AgNP/Bi2Fe4O9 composite, Appl. Catal., B 227 (2018) 548–556, https://doi.org/10.1016/j.apcatb.2018.01.047.

[13] W. Han, W. Wang, J. Fan, R. Jia, X. Yang, T. Wu, Q. Wu, A novel Ag/ZnO core-shell structure for efficient sterilization synergizing antibiotics and subsequently removing residuals, Green, Energy Environ. (2022), https://doi.org/10.1016/j.gee.2022.07.004.

[14] G.R. Tortella, O. Rubilar, N. Durán, M.C. Diez, M. Martínez, J. Parada, A.B. Seabra, Silver nanoparticles: Toxicity in model organisms as an overview of its hazard for human health and the environment, J. Hazard. Mater. 390 (2020), 121974, https://doi.org/10.1016/j.jhazmat.2019.121974.

[15] M. Vincent, P. Hartemann, M. Engels-Deutsch, Antimicrobial applications of copper, Int. J. Hyg. Environ. Health 219 (2016) 585–591, https://doi.org/10.1016/j.ijheh.2016.06.003.

[16] L.P. Arendsen, R. Thakar, A.H. Sultan, The use of copper as an antimicrobial agent in health care, including obstetrics and gynecology, Clin. Micro Rev. 32 (2019) e00125–00118, https://doi.org/10.1128/cmr.00125-18.

[17] T.M. Gross, J. Lahiri, A. Golas, J. Luo, F. Verrier, J.L. Kurzejewski, D.E. Baker, J. Wang, P.F. Novak, M.J. Snyder, Copper-containing glass ceramic with high antimicrobial efficacy, Nat. Commun. 10 (2019) 1979–1986, https://doi.org/10.1038/s41467-019-09946-9.

[18] S.M. Imani, L. Ladouceur, T. Marshall, R. Maclachlan, L. Soleymani, T.F. Didar, Antimicrobial nanomaterials and coatings: current mechanisms and future perspectives to control the spread of viruses including SARS-CoV-2, ACS Nano 14 (2020) 12341–12369, https://doi.org/10.1021/acsnano.0c05937.

[19] M.E. Villanueva, A.Md.R.. Diez, J.A. Gonzále, C.J. Pérez, M. Orrego, L. Piehl, S. Teve, G.J. Copello, Antimicrobial activity of starch hydrogel incorporated with copper nanoparticles, ACS Appl. Mater. Interfaces, 8, 2016: 16280–16288. http://doi.org/10.1021/acsami.6b02955.

[20] X. Wang, H. Dong, Q. Zeng, Q. Xia, L. Zhang, Z. Zhou, Reduced iron-containing clay minerals as antibacterial agents, Environ. Sci. Technol. 51 (2017) 7639–7647, https://doi.org/10.1021/acs.est.7b00726.

[21] S. Kang, J. Choi, G.Y. Park, H.R. Kim, J. Hwang, A novel and facile synthesis of Ag-doped TiO2 nanofiber for airborne virus/bacteria inactivation and VOC elimination under visible light, Appl. Surf. Sci. 599 (2022) 153930–153942, https://doi.org/10.1016/j.apsusc.2022.153930.

[22] E. Evgenidou, Z. Chatzisalata, A. Tsevis, K. Bourikas, P. Torounidou, D. Sergelidis, A. Koltsakidou, D.A. Lambropoulou, Photocatalytic degradation of a mixture of eight antibiotics using Cu-modified TiO2 photocatalysts: Kinetics, mineralization, antimicrobial activity elimination and disinfection, J. Environ. Chem. Eng. 9 (2021) 105295–105309, https://doi.org/10.1016/j.jece.2021.105295.

[23] H. Wang, M. Yu, S. Cui, L. Dong, S. Wang, S. Wei, H. Feng, S. Chen, Branched CuO-Co3O4 nanowires coated with carbon on Cu foam for water sterilization, 105629-101056, J. Environ. Chem. Eng. 9 (2021), https://doi.org/10.1016/j.jece.2021.105629.

[24] K. Wenderich, G. Mul, Methods, mechanism, and applications of photodeposition in photocatalysis: a review, Chem. Rev. 116 (2016) 14587–14619, https://doi.org/10.1021/acs.chemrev.6b00327.

[25] G. Zhang, H. Wu, D. Chen, N. Li, Q. Xu, H. Li, J. He, J. Lu, A mini-review on ZnIn2S4-Based photocatalysts for energy and environmental application, Green. Energy Environ. 7 (2022) 176–204, https://doi.org/10.1016/j.gee.2020.12.015.

[26] R. Yang, L. Mei, Y. Fan, Q. Zhang, R. Zhu, R. Amal, Z. Yin, Z. Zeng, ZnIn2S4-based photocatalysts for energy and environmental applications, Small Methods 5 (2021) 2100887–2100946, https://doi.org/10.1002/smtd.202100887.

[27] S. Maoa, J.W. Shi, G. Suna, D. Ma, C. He, Z. Pu, K. Song, Y. Cheng, Au nanodots@thiol-UiO66@ZnIn2S4 nanosheets with significantly enhanced visible-light photocatalytic H2 evolution: The effect of different Au positions on the transfer of electron-hole pairs, Appl. Catal., B 282 (2021) 119550–119559, https://doi.org/10.1016/j.apcatb.2020.119550.

[28] Z.-T. Hu, Z.-Y. Jin, S.-Y. Gong, X. Wei, J. Zhao, M. Hu, J. Zhao, Z. Chen, Z. Pan, X. Li, Supermagnetic Mn-substituted ZnFe2O4 with AB-site hybridization for the ultra-effective catalytic degradation of azoxystrobin, Catal. Sci. Technol. 12 (2022) 3137–3147, https://doi.org/10.1039/d2cy00142j.

[29] Z.T. Hu, W.H. Xing, S.Y. Gong, T. Sun, C. Wang, M. Hu, J. Zhao, Z. Pan, W. Chen, Z. Chen, X. Li, Flower-like ZnIn2S4 microspheres with highly efficient catalytic activity for visible-light-driven sulfamethoxazole photodegradation, Colloids Surf., A 643 (2022) 128779–128788, https://doi.org/10.1016/j.colsurfa.2022.128779.

[30] Z. Cui, S. Song, H. Liu, Y. Zhang, F. Gao, T. Ding, Y. Tian, X. Fan, X. Li, Synergistic effect of Cu+ single atoms and Cu nanoparticles supported on alumina boosting water-gas shift reaction, Appl. Catal., B 313 (2022), https://doi.org/10.1016/j.apcatb.2022.121468.

[31] S. Lu, J. Zhang, H. Meng, X. Qin, J. Huang, Y. Liang, F.-S. Xiao, Catalytic direct dehydrogenation of ethyl lactate to produce ethyl pyruvate over a synergetic Cu0/Cu+ interface, Appl. Catal., B 325 (2023), https://doi.org/10.1016/j.apcatb.2022.122329.

[32] N. Luo, T. Montini, F. Fan, J. Zhang, P. Fornasiero, T. Hou, W. Nie, J. Lu, J. Liu, M. Heggen, M. Wang, S. Jin, F. Wang, Visible-light-driven coproduction of diesel precursors and hydrogen from lignocellulose-derived methylfurans, Nat. Energy 4 (2019) 575–584, https://doi.org/10.1038/s41560-019-0403-5.

[33] H. Li, H. Ji, J. Liu, W. Liu, F. Li, Z. Shen, Interfacial modulation of ZnIn2S4 with high active Zr-S4 sites for boosting photocatalytic activation of oxygen and degradation of emerging contaminant, Appl. Catal., B 328 (2023), https://doi.org/10.1016/j.apcatb.2023.122481.

[34] Q. Lin, Y.H. Li, M.Y. Qi, J.Y. Li, Z.R. Tang, M. Anpo, Y.M.A. Yamada, Y.J. Xu, Photoredox dual reaction for selective alcohol oxidation and hydrogen evolution over nickel surface-modified ZnIn2S4, Appl. Catal., B 271 (2020) 118946–118952, https://doi.org/10.1016/j.apcatb.2020.118946.

[35] C.C. Hu, C.Y. Wang, M.C. Tsai, R.L.G. Lecaros, W.S. Hung, H.A. Tsai, K.R. Lee, J.Y. Lai, Polyimide/Cu-doped TiO2 Janus membranes for direct capture and photocatalytic reduction of carbon dioxide from air, Chem. Eng. J. 450 (2022) 138008–138018, https://doi.org/10.1016/j.cej.2022.138008.

[36] S. Liu, X. Zhou, C. Yang, C. Wei, Y. Hu, Cu atoms on UiO-66-NH2/ZnIn2S4 nanosheets enhance photocatalytic performance for recovering hydrogen energy from organic wastewater treatment, Appl. Catal., B 330 (2023), https://doi.org/10.1016/j.apcatb.2023.122572.

[37] Y. Qin, H. Li, J. Lu, Y. Feng, F. Meng, C. Ma, Y. Yan, M. Meng, Synergy between van der waals heterojunction and vacancy in ZnIn2S4/g-C3N4 2D/2D photocatalysts for enhanced photocatalytic hydrogen evolution, Appl. Catal., B 277 (2020) 119254–119263, https://doi.org/10.1016/j.apcatb.2020.119254.

[38] J. Qiu, M. Li, L. Yang, J. Yao, Facile construction of three-dimensional netted ZnIn2S4 by cellulose nanofibrils for efficiently photocatalytic reduction of Cr(VI, Chem. Eng. J. 375 (2019) 121990–121998, https://doi.org/10.1016/j.cej.2019.121990.

[39] J. Wang, D. Wang, X. Zhang, C. Zhao, M. Zhang, Z. Zhang, J. Wang, An anti-symmetric dual (ASD) Z-scheme photocatalytic system: (ZnIn2S4/Er3+: Y3Al5O12@ZnTiO3/CaIn2S4) for organic pollutants degradation with simultaneous hydrogen evolution, Int. J. Hydrog. Energy 44 (2019) 6592–6607, https://doi.org/10.1016/j.ijhydene.2019.01.214.

[40] Y. Zhao, G. Zuo, Y. Wang, W.L. Teo, A. Xie, Y. Guo, Y. Dai, W. Zhou, D. Jana, Q. Xian, W. Dong, Ultrathin ZnIn2S4 nanosheets anchored on Ti3C2TX MXene for

[41] photocatalytic H2, Evol., Angew. Chem. Int. Ed. 59 (2020) 11287–11292, https://doi.org/10.1002/anie.202002136.

[41] E. Borfecchia, K.A. Lomachenko, F. Giordanino, H. Falsig, P. Beato, A.V. Soldatov, S. Bordiga, C. Lamberti, Revisiting the nature of Cu sites in the activated Cu-SSZ-13 catalyst for SCR reaction, Chem. Sci. 6 (2015) 548–563, https://doi.org/10.1039/c4sc02907k.

[42] K.V. Karthik, A.V. Raghu, K.R. Reddy, R. Ravishankar, M. Sangeeta, N.P. Shetti, C.V. Reddy, Green synthesis of Cu-doped ZnO nanoparticles and its application for the photocatalytic degradation of hazardous organic pollutants, Chemosphere 287 (2022) 132081–132090, https://doi.org/10.1016/j.chemosphere.2021.132081.

[43] H. Safajou, M. Ghanbari, O. Amiri, H. Khojasteh, F. Namvar, S. Zinatloo-Ajabshir, M. Salavati-Niasari, Green synthesis and characterization of RGO/Cu nanocomposites as photocatalytic degradation of organic pollutants in waste-water, Int. J. Hydrog. Energy 46 (2021) 20534–20546, https://doi.org/10.1016/j.ijhydene.2021.03.175.

[44] W.B. Widayatno, G. Guan, J. Rizkiana, J. Yang, X. Hao, A. Tsutsumi, A. Abudula, Upgrading of bio-oil from biomass pyrolysis over Cu-modified β-zeolite catalyst with high selectivity and stability, Appl. Catal., B 186 (2016) 166–172, https://doi.org/10.1016/j.apcatb.2016.01.006.

[45] D. Zeng, Z. Lu, X. Gao, B. Wu, W.J. Ong, Hierarchical flower-like ZnIn2S4 anchored with well-dispersed Ni12P5 nanoparticles for high-quantum-yield photocatalytic H2 evolution under visible light, Catal. Sci. Technol. 9 (2019) 4010–4016, https://doi.org/10.1039/c9cy00904a.

[46] G. Cui, X. Zhang, H. Wang, Z. Li, W. Wang, Q. Yu, L. Zheng, Y. Wang, J. Zhu, M. Wei, ZrO2-x modified Cu nanocatalysts with synergistic catalysis towards carbon-oxygen bond hydrogenation, Appl. Catal., B 280 (2021) 119406–119416, https://doi.org/10.1016/j.apcatb.2020.119406.

[47] T. Zhu, X. Ye, Q. Zhang, Z. Hui, X. Wang, S. Chen, Efficient utilization of photogenerated electrons and holes for photocatalytic redox reactions using visible light-driven Au/ZnIn2S4 hybrid, J. Hazard. Mater. 367 (2019) 277–285, https://doi.org/10.1016/j.jhazmat.2018.12.093.

[48] C.L. Tan, M.Y. Qi, Z.R. Tang, Y.J. Xu, Cocatalyst decorated ZnIn2S4 composites for cooperative alcohol conversion and H2 evolution, Appl. Catal., B 298 (2021) 120541–120549, https://doi.org/10.1016/j.apcatb.2021.120541.

[49] Z. Liu, S. Fan, X. Li, Z. Niu, J. Wang, C. Bai, J. Duan, M.O. Tadé, S. Liu, Synergistic effect of single-atom Cu and hierarchical polyhedron-like Ta3N5/CdIn2S4 S-scheme heterojunction for boosting photocatalytic NH3 synthesis, Appl. Catal., B 327 (2023), https://doi.org/10.1016/j.apcatb.2023.122416.

[50] J. Chen, Y. Tang, S. Wang, L. Xie, C. Chang, X. Cheng, M. Liu, L. Wang, L. Wang, Ingeniously designed Ni-Mo-S/ZnIn2S4 composite for multi-photocatalytic reaction systems, Chin. Chem. Lett. 33 (2022) 1468–1474, https://doi.org/10.1016/j.cclet.2021.08.103.

[51] M. Cao, F. Yang, Q. Zhang, J. Zhang, L. Zhang, L. Li, X. Wang, W.L. Dai, Facile construction of highly efficient MOF-based Pd@UiO-66-NH2@ZnIn2S4 flower-like nanocomposites for visible-light-driven photocatalytic hydrogen production, J. Mater. Sci. Technol. 76 (2021) 189–199, https://doi.org/10.1016/j.jmst.2020.11.028.

[52] J. He, J. Cheng, I.M.C. Lo, Green photocatalytic disinfection of real sewage: efficiency evaluation and toxicity assessment of eco-friendly TiO2-based magnetic photocatalyst under solar light, Water Res. 190 (2021) 116705–116716, https://doi.org/10.1016/j.watres.2020.116705.

[53] Z. Jiang, B. Wang, Y. Lid, H.S. Chan, H. Sun, T. Wang, H. Lia, S. Yuana, M.K. H. Leunge, A. Lud, P.K. Wong, Solar-light-driven rapid water disinfection by ultrathin magnesium titanate/carbon nitride hybrid photocatalyst: Band structure analysis and role of reactive oxygen species, Appl. Catal., B 257 (2019) 117898–117906, https://doi.org/10.1016/j.apcatb.2019.117898.

[54] H. Zhang, W. Wei, M. Huang, Z. Umar, Y. Feng, Definition of a family of nonmobile colistin resistance (NMCR-1) determinants suggests aquatic reservoirs for MCR-4, Adv. Sci. 6 (2019) 1900038–1900052, https://doi.org/10.1002/advs.201900038.

[55] D.P. Linklater, V.A. Baulin, X.L. Guevel, J.B. Fleury, E. Hanssen, T.H.P. Nguyen, S. Juodkazis, G. Bryant, R.J. Crawford, P. Stoodley, E.P. Ivanova, Antibacterial action of nanoparticles by lethal stretching of bacterial cell membranes, Adv. Mater. 32 (2020) 2005679–2005693, https://doi.org/10.1002/adma.202005679.

[56] J. Du, S. Ma, H. Liu, H. Fu, L. Li, Z. Li, Y. Li, J. Zhou, Uncovering the mechanism of novel AgInS2 nanosheets/TiO2 nanobelts composites for photocatalytic remediation of combined pollution, Appl. Catal., B 259 (2019) 118062–118076, https://doi.org/10.1016/j.apcatb.2019.118062.

[57] J. Sun, L. Guo, Q. Li, Y. Zhao, M. Gao, Z. She, G. Wang, Structural and functional properties of organic matters in extracellular polymeric substances (EPS) and dissolved organic matters (DOM) after heat pretreatment with waste sludge, Bioresour. Technol. 219 (2016) 614–623, https://doi.org/10.1016/j.biortech.2016.08.042.

[58] G. Xiao, X. Zhang, W. Zhang, S. Zhang, H. Su, T. Tan, Visible-light-mediated synergistic photocatalytic antimicrobial effects and mechanism of Ag-nanoparticles@chitosan–TiO2 organic–inorganic composites for water disinfection, Appl. Catal., B, 170- 171 (2015) 255–262, https://doi.org/10.1016/j.apcatb.2015.01.042.

[59] Y. Hou, X. Li, D. Zhao, G. Chen, C.L. Raston, Role of hydroxyl radicals and mechanism of Escherichia coli inactivation on Ag/AgBr/TiO2 nanotube array electrode under visible light irradiation, Environ. Sci. Technol. 46 (2012) 4042–4050, https://doi.org/10.1021/es204079d.

[60] A. Parastaev, V. Muravev, E.H. Osta, A.J.Fv Hoof, T.F. Kimpel, N. Kosinov, E.J. M. Hensen, Boosting CO2 hydrogenation via size-dependent metal–support interactions in cobalt/ceria-based catalysts, Nat. Catal. 3 (2020) 526–533, https://doi.org/10.1038/s41929-020-0459-4.